Advective transport in percolation clusters

Matthew E. Rhodes* and Martin J. Blunt†
Department of Earth Science and Engineering, Imperial College London, South Kensington, London, United Kingdom
(Received 27 June 2006; published 25 January 2007)

We simulate advective transport in bond percolation clusters at the critical point. We compute the histogram of flow speeds in each bond of the backbone and find the multifractal spectrum for two-dimensional lattices with linear dimension $L \leqslant 2000$ and in three dimensions for $L \leqslant 250$. We demonstrate that in the limit of large systems all the negative moments of the velocity distribution become ill-defined. However, to model transport, the velocity histogram should be weighted by the flux to obtain a well-defined mean travel time. Finally, we use continuous time random walk theory to demonstrate that anomalous transport is observed whose characteristics can be related to the multifractal properties of the system.

DOI: 10.1103/PhysRevE.75.011124 PACS number(s): 05.40.−a, 05.45.Df, 47.53.+n

I. INTRODUCTION

The static and dynamic properties of fractal media have been the subject of numerous analytical and numerical treatments with a variety of applications including turbulence [1], forest fires [2], dielectric breakdown [3], growth properties [4], viscous fingering [5], and flow in heterogeneous porous media [6,7]. One exemplar of a fractal structure, which has been used as an analogue for porous media, is a percolation cluster at its threshold. Analyzing flow in such structures has provided insight into the transport physics of real-life systems [2,7]. Many of the early studies into these networks computed the moments of the resultant velocity distributions [8–10] or found average macroscopic properties such as conductivity or permeability [11]. In this work, we are interested in using these distributions to model advective-dominated transport. Lopez *et al.* [12] proposed scaling laws for the breakthrough curves for advective transport between wells in two dimensions. Here we extend the previous studies on multifractal spectra in two-dimensional percolation clusters [10] to larger system sizes and to three dimensions. We also relate the moments of the velocity distribution to computed transport behavior.

The distribution of bond velocities, $P(V)$, within a threshold percolation cluster has been shown to be multifractal [13,14]. We define this $P(V)dV$ as the probability that a given bond, ij has a velocity V_{ij} in the range $V-dV/2 \leqslant V_{ij} < V+dV/2$. For large L the number of bonds $n(V)$ with velocity, $V \sim L^{-\alpha}$ [15], in a logarithmic increment $d \ln V$, will scale with an infinite set of exponents $f(\alpha)$ with the form

$$n(V)d\ln(V) \sim L^{f(\alpha)}d\ln V, \tag{1}$$

where $f(\alpha)=\ln[n(V)]/\ln(L)$ and $\alpha=-\ln(V)/\ln(L)$ [13,16]. The moments $M(q)$ of this velocity distribution which we define as

$$M(q) \equiv \left\langle \sum_{\forall ij} V_{ij} \right\rangle = \frac{1}{N_r} \sum_{\forall r} \sum_{\forall V_{ij} \neq 0} V_{ij}, \tag{2}$$

where N_r is the number of realizations, do not follow a constant gap length scaling and require an infinite set of exponents $\tau(q)=[f(\alpha^*)-q\alpha^*]_{q=df/d\alpha|_{\alpha=\alpha^*}}$ to characterize [15,16].

The flow velocity is equivalent to the current in a random resistor network. However, for transport, it is not correct to weight the velocity distribution uniformly between bonds. This would imply that a particle moving in the flow field is equally likely to reside in each bond in the backbone regardless of its velocity. Instead, the histogram of particle velocities must be weighted by the flux (velocity) [17].

As we weight our $f(\alpha)$ spectra with flux, before we use it to find the travel time moments in our transport simulations we must define a new $f_v(\alpha)$,

$$f_v(\alpha) = \frac{\ln[Vn(V)]}{\ln(L)}, \tag{3}$$

where

$$f_v(\alpha) = f(\alpha) - \alpha \tag{4}$$

and a new flux weighted velocity distribution $P_v(V)$,

$$P_v\left(V - \frac{dV}{2} \leqslant V_{ij} < V + \frac{dV}{2}\right)dV = \frac{n(V)V}{N_{V\neq 0}}\, d\ln V, \tag{5}$$

where $N_{V\neq 0}$ is the number of nonzero velocity bonds in the system. This definition helps resolve the debate in the literature over the negative moments of the velocity distribution [10,18–20]. It has been argued that the moments, $M(q)$, only exist for $q \geqslant q_c$ where $q_c=0$. This implies that the mean transit time ($q=-1$) is ill-defined since particles will be stuck for arbitrarily long periods in a finite fraction of low velocity bonds. However, using flux weighting q_c becomes -1 implying that a mean transit time is defined although the standard deviation ($q=-2$) is not, suggesting that the effective dispersion coefficient of the transport will diverge in the limit as $t \to \infty$. This is anomalous transport that has been studied in the context of continuous time random walk (CTRW) theory [21–23]. Our simulation results, shown later, are indeed consistent with $q_c=0$ or -1 for uniform and flux weighting re-

*Electronic address: matthew.rhodes@imperial.ac.uk
†Electronic address: m.blunt@imperial.ac.uk

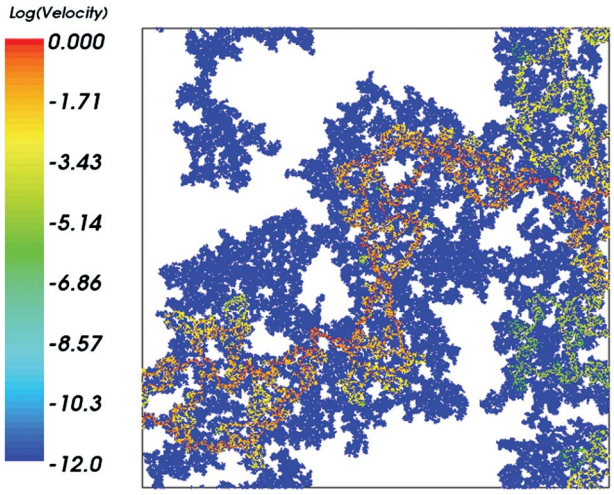

FIG. 1. (Color online) A two-dimensional percolation cluster at its critical point with linear dimension $L=1000$. The colors indicate the logarithm of the absolute velocity in the bonds. For illustrative purposes dead-ends are shown with a small but finite velocity of 1×10^{-12} though in the simulations they carry no flow.

spectively and we show that particle transport can be predicted using CTRW and the measured $f_v(\alpha)$ spectrum.

II. METHOD

We investigated flow on square and cubic bond percolation clusters at their critical point. We modified the algorithm in Ref. [20] to extract a threshold percolation cluster in which the bonds are connected together at the nodes. We labeled each node, i, with an index from 0 to $N-1$, where N was the total number of nodes. We then visited each of these nodes in turn connecting them to their nearest neighbor j

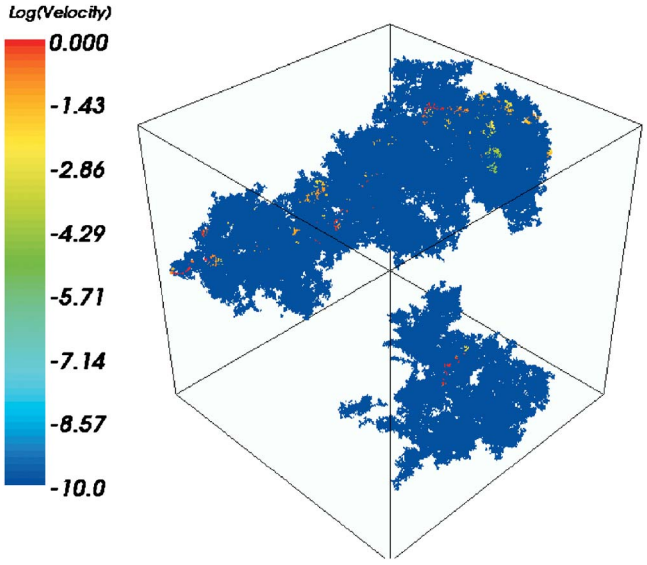

FIG. 2. (Color online) A three-dimensional percolation cluster at its critical point with linear dimension $L=200$. The colors indicate the logarithm of the absolute velocity in the bonds. Dead-ends are set to a small but finite velocity of 1×10^{-10}.

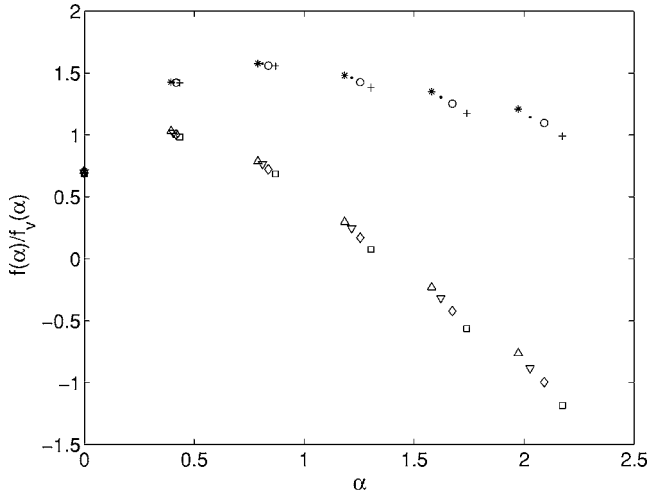

FIG. 3. Plot showing the uniform (upper curves) and flux-weighted (lower curves) $f(\alpha)$ spectra in two dimensions for systems of size; upper curves, $L=2000$ (asterisks), $L=1000$ (dots), $L=500$ (open circles), $L=250$ (crosses); lower curves, $L=2000$ (triangles), $L=1000$ (inverted triangles), $L=500$ (diamonds), and $L=250$ (squares).

with a bond of unit length if $j>i$ and a randomly generated number, p_j between 0 and 1 was less than or equal to the occupation probability p. We set the value of p to be 0.5 and 0.2488 in two and three dimensions, respectively, i.e., the critical values of p presented in the literature [2]. In two dimensions the two y axes were periodic, i.e., a point on one y boundary could connect to a point on the other boundary with the same x coordinate, while in three dimensions the bounding y and z planes were periodic. We then sorted the system into clusters using a tree-based clustering algorithm [24,25], determined if a spanning cluster existed, extracted it from the system if it did or discarded the grid if it did not. The flow field was then determined by imposing an external pressure field on the two x boundaries assuming flux continuity and Darcy's law at each node:

$$\sum_{\forall j} K_{ij}(P_i - P_j) = 0 \quad \forall\, i, \tag{6}$$

where P is the pressure and i and j label nodes connected by bond ij having a conductance K_{ij} which we assumed to be of unit magnitude.

We then obtained a system of linear equations which we solved by inverting the resulting sparse matrix using an algebraic multigrid solver [26]. Using this solution we calculated the flux in each bond. If the maximum bond velocity was less than the total inlet velocity there was no single bond present in the lattice able to carry the entire flux of the system. These bonds are known in the literature as red bonds and are a key criteria for criticality in percolation clusters [2]. These realizations were thus regarded to be anomalies due to correlations in the random number generator and above the critical point. These grids were subsequently rejected and the algorithm repeated.

Visual examples of the velocity field calculated for two critical percolation clusters in two and three dimensions are

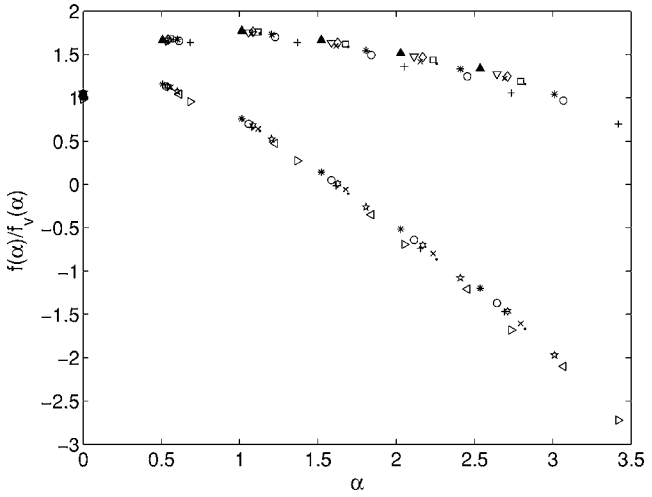

FIG. 4. Plot showing the uniform (upper curves) and flux-weighted (lower curves) $f(\alpha)$ spectra in three dimensions; upper curves, $L=250$ (triangles), $L=200$ (inverted triangles), $L=175$ (diamonds), $L=150$ ($\times$), $L=125$ (squares), $L=100$ (dots), $L=75$ (asterisks), $L=50$ (open circles), $L=25$ (crosses); lower curves, $L=250$ (asterisks), $L=200$ (open circles), $L=175$ (crosses), $L=150$ (six pointed stars), $L=125$ ($\times$), $L=100$ (dots), $L=75$ (five pointed stars), $L=50$ (right-pointing triangles), $L=25$ (left-pointing triangles).

shown in Figs. 1 and 2 with the potential gradient applied from left to right and top to bottom, respectively. The uniform $f(\alpha)$ and flux weighted $f_v(\alpha)$ spectra were then found from the logarithmic binning of this velocity distribution [8,15].

We also modeled transport in the advective limit by tracking the movement of 10^5 random walkers within the system. Each particle was assigned to a node on a line or plane that was one-quarter of the way into the structure with a probability weighted by the flux leaving that node. We then monitored the progress of each walker from node to node using a generalized semianalytical particle tracking algorithm [27,28]. Each transition occurred in an advective time $t_a = L_{bij}/V_{ij}$ where L_{bij} is the $i-j$th bond length taken as 1. We assumed that complete mixing occurred at each node with the probability of arriving at a nearest neighbor, p_{ij} being proportional to the flux in the corresponding bond ij [27,28]:

$$p_{ij} = \frac{V_{ij}}{\sum_{\forall ij} V_{ij}} \quad \text{for } V_{ij} > 0, \quad p_{ij} = 0 \text{ otherwise}, \tag{7}$$

where $V_{ij} > 0$ defines a flux leaving node i heading in the direction of node j. We recorded the total time for each particle to transit the system, the average displacement $\bar{l}(t)$ and the standard deviation of the concentration plume $\sigma(t)$ for 100 different realizations.

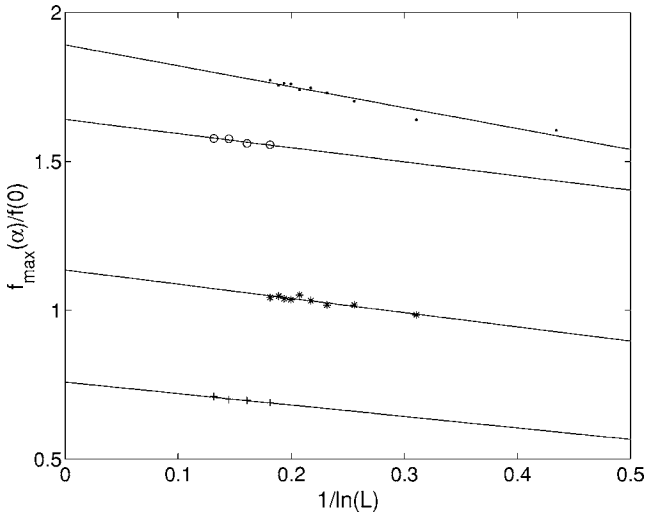

FIG. 5. A plot showing $f_{\max}(\alpha)$ and $f(0)$ vs $1/\ln L$ for all the systems investigated. The dots represent the plot of $f_{\max}(\alpha)$ in three dimensions; the open circles, $f_{\max}(\alpha)$ in two dimensions; the asterisks, $f(0)$ in three dimensions; and the crosses, $f(0)$ in two dimensions.

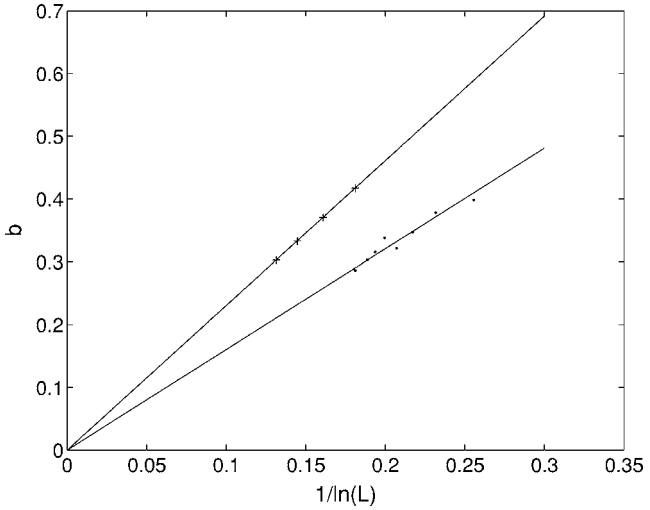

FIG. 6. Plot showing the exponent b of a linear late time fit of the $f(\alpha)$ spectra vs $1/\ln(L)$ in both two (crosses) and three dimensions (dots).

III. RESULTS

In Sec. III A we show the flux weighted $f_v(\alpha)$ and traditional $f(\alpha)$ plots and compare their salient features to those presented in the literature. In Sec. III B we discuss the scaling of the quiet side ($q<0$) of the velocity spectrum while in Sec. III C we look at the results of the transport simulations and relate these to CTRW theory.

A. Multifractal spectra

In Figs. 3 and 4 we show the uniform and flux weighted spectra in both two and three dimensions, respectively. We validate our work by extrapolating the plots of $f_{\max}(\alpha) \equiv f(\alpha)|_{df/d\alpha=0}$ and $f(0)$ vs $1/\ln L$ in Fig. 5 to the 0 of the abscissa. It is known that in the limit of $L \to \infty$ these plots will give the fractal dimension of the backbone (d_b) and the red bonds (d_{rb}), respectively [5,16]. From our work we found values of 1.64 ± 0.01 and 1.89 ± 0.03 for the fractal dimension of the backbone in two and three dimensions, respectively,

TABLE I. Table showing the best-fit value of β_v for different system sizes in two dimensions.

	β_v			
L	500	1000	1500	2000
V	1.4±0.3	1.3±0.2	1.3±0.2	1.3±0.2
$\sigma(t)$	1.6±0.2	1.6±0.2	1.6±0.2	1.6±0.2
$C(t)$	1.7±0.2	1.7±0.2	1.7±0.2	1.7±0.2

which corresponded extremely well with the current best direct numerical estimates of 1.64 and 1.88 [29,30]. We were also able to get an excellent match of 0.76±0.01 and 1.13±0.01 for the values of d_{rb} in two and three dimensions as compared to the values of 0.75 and 1.13 that are in the literature [2,31].

B. The low velocity (quiet side) of the flux distribution

The low velocity side of the velocity distribution is now widely accepted as a power law in velocity of the form $P(V)dV \sim V^{b-1}dV = V^b d \ln V$ where $b \geqslant 0$ [20,32]. This leads to $f(\alpha) = -b\alpha$ for large α, with $q_c = -b$. It has been suggested that this power-law exponent scales with system size as [18,20]

$$b(L) = b_\infty + \frac{D}{\ln L} + \sigma(L), \tag{8}$$

where b_∞ is the scaling in the infinite limit and $\sigma(L)$ is a correction factor that decays faster than $1/\ln L$ [10]. It has been proposed that this exponent (b_∞) could have a finite value of about 0.25 [32] while Ref. [20] concluded from numerical simulations that this value is 0. This was later corroborated by Barthelemy *et al.* [10] who also obtained a value of 0 using a larger range of system sizes ($L \leqslant 1000$).

We estimate a value of b from the slope of a linear fit to $f(\alpha)$ for $\alpha > 1$. In Fig. 6, b is plotted as a function of $1/\ln L$ in two and three dimensions. Extrapolating $L \to \infty$ indicates that $b_\infty = 0 \pm 0.001$ consistent with the results of Ref. [10] in two dimensions. However if we consider flux-weighted distributions $b_{v\infty} = b_\infty + 1 = 1$. This indicates that for transport the mean travel time is defined.

C. Transport simulations

According to CTRW theory the probability that a particle will move between two nearest neighbor nodes, in a time interval t to $t+dt$ is defined as $\psi(t)dt$ [21]. If, at late times, this function can be approximated by a power law in time, we can write $\psi(t) \sim t^{-1-\beta}$ with $\beta < 2$ describing transport which is anomalous [33,34]. For $1 < \beta < 2$ it can be shown [34–36] that the average displacement of the plume, $\bar{l}(t)$, scales linearly with time with a finite mean transition time while the standard deviation of the plume location, $\sigma(t) \sim t^{(3-\beta)/2}$ indicating a divergent dispersion coefficient in the limit of infinite time, while the concentration $C(t)$ arriving at an extraction line/production well or plane scales as $t^{-1-\beta}$. For $0 < \beta < 1$, $\bar{l}(t)$ and $\sigma(t) \sim t^\beta$, while $C(t) \sim t^{-1-\beta}$. For $\beta > 2$, transport approaches the Gaussian limit with $C(t) \sim e^{-\lambda t}$, $\bar{l}(t) \sim t$, and $\sigma(t) \sim t^{1/2}$ with λ being a medium specific parameter.

TABLE II. Table showing the value of β_v for different system sizes in three dimensions.

	β_v				
L	50	75	100	150	200
V	1.4±0.3	1.4±0.3	1.4±0.2	1.3±0.2	1.3±0.2
$\sigma(t)$	1.9±0.3	1.9±0.3	1.9±0.2	1.8±0.2	1.8±0.2
$C(t)$	1.5±0.2	1.5±0.2	1.4±0.2	1.4±0.2	1.4±0.2

1. Relating the transport and the velocity distributions

We now derive a relationship between the transit time and the velocity distribution. It has already been established that $P(V) \sim V^{b-1}$. We also know that the transition time $t \sim 1/V$ and $dV \sim t^{-2}dt$, so substituting for V we can write

$$P(V)dV \sim V^{b-1}dV \sim \left(\frac{1}{t}\right)^{b-1} t^{-2}dt \sim t^{-(b+1)}dt. \tag{9}$$

Therefore by comparison with the scaling of $\psi(t)$ and $P(V)$, we get

$$\beta \equiv b \tag{10}$$

while for $P_v(V)$, we find that

$$P_v(V)dV \sim V \times V^{b-1}dV \sim \left(\frac{1}{t}\right)^{b} t^{-2}dt \sim t^{-(b+2)}dt, \tag{11}$$

thus

$$\beta_v \equiv b + 1 \equiv b_v. \tag{12}$$

We conducted 100 numerical transport simulations on several different realizations of spanning percolation clusters for each lattice size of interest. We then tabulated and binned all the results in two and three dimensions and used this to estimate the values of β_v that we show in Tables I and II, respectively. These estimates were obtained from (i) the $f_v(\alpha)$ plot where we find as best-fit slope, b_v for $\alpha > 1$ using the fact that $\beta_v = b_v$; (ii) the standard deviation of the particle location as a function of time given by

$$\sigma(t) = \sqrt{\sum_{i=1}^{N_p} \frac{[l_i(t) - \bar{l}(t)]^2}{N_p}}, \tag{13}$$

where the sum is over all N_p particles, $l_i(t)$ is the displacement of the particle from the origin in the average flow (x) direction, $\bar{l}(t)$ is the average displacement of the plume given by

$$\bar{l}(t) = \sum_{i=1}^{N_p} \frac{l_i(t)}{N_p} \tag{14}$$

and β_v is a best-fit to $\sigma(t) \sim t^{(3-\beta_v)/2}$ at late time: one example is shown in Fig. 7; and (iii) from the outlet concentration,

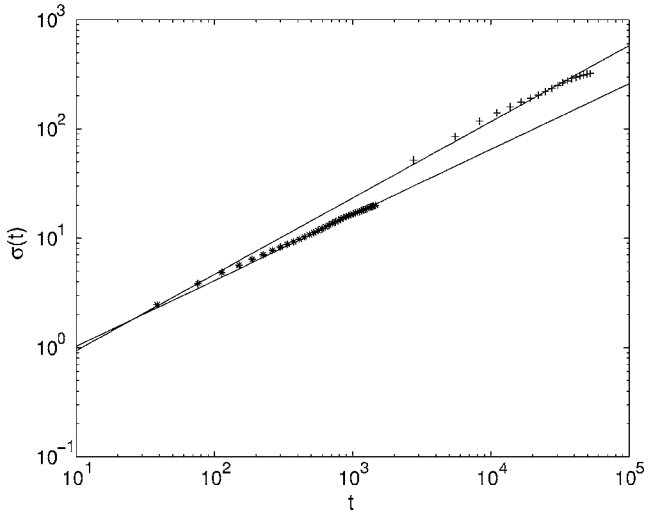

FIG. 7. Figure showing the scaling of the standard deviation of the plume displacement with respect to time in two dimensions for a system of size $L=2000$ (crosses) and in three dimensions for a system of size $L=200$ (asterisks).

$C(t)$, with β_v as a best fit to $C(t) \sim t^{-1-\beta_v}$ at late times with $C(t)dt$ being proportional to the number of particles leaving the system in a time dt. In all cases we find that $\bar{l}(t) \sim t$ consistent with $\beta_v > 1$.

The values of β_v estimated from the velocity distribution and the transport simulations are broadly consistent. However, relating β_v and b_v assumes that the bond velocities are spatially uncorrelated. This is not necessarily the case for percolation networks that have a hierarchical clustered structure which may require a general $\psi(s,t)$ [37] to obtain a closer consistency between the two distributions. In two dimensions the computed β_v from transport is larger than estimated from the velocity distribution, indicating less anomalous transport. In three dimensions, the value of β_v

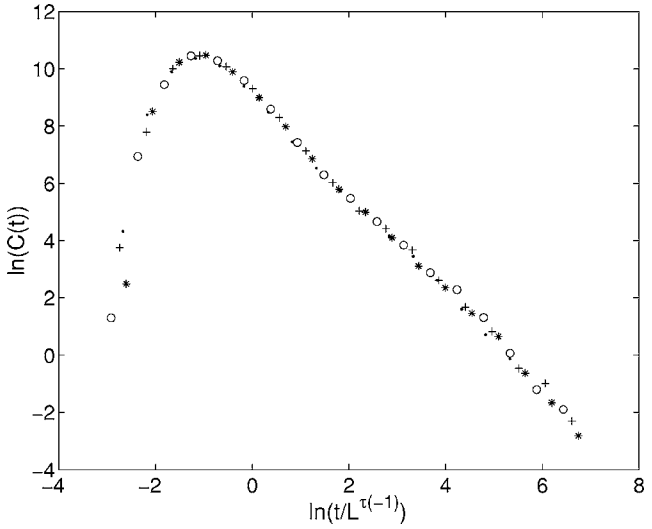

FIG. 8. Figure showing the universal scaling of the outlet concentration $C(t)$ for different system sizes $L=2000$ (dots), $L=1500$ (asterisks), $L=1000$ (open circles), and $L=500$ (crosses) in two dimensions.

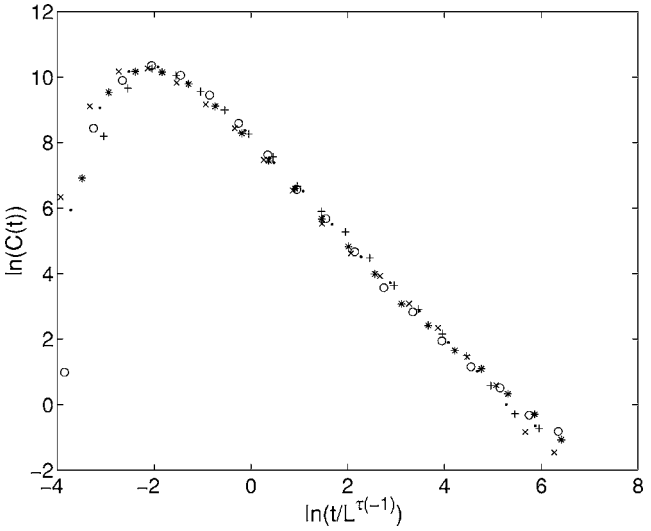

FIG. 9. Figure showing the universal scaling of the outlet concentration $C(t)$ for different system sizes $L=200$ (×), $L=150$ (dots), $L=100$ (asterisks), $L=75$ (open circles), and $L=50$ (crosses) in three dimensions.

determined from $C(t)$ is consistent with the value from the velocity distribution, but the dispersion is less anomalous.

2. Universal scaling of the transit time curves

From a practical standpoint a key transport measure is $C(t)$ since this quantifies the outlet flux of the particles, which for contaminant transport is equivalent to the rate at which pollutant can be removed from the system. In this section we find a universal curve of $C(t)$ for transport in different system sizes. These curves when denormalized for a system of interest could be used as a first estimate for the transit distribution without having to perform any numerical experiments.

As in all our simulations we use the same number of particles regardless of L, there will be no functional dependence of $\int_0^\infty C(t)dt$ with the system size. This, though, is not true for the mean transit time of $C(t)$, t_m. It can be shown that t_m is controlled by the -1th moment of the velocity distribution. The time taken for a single particle to transit the system t_s is given by

$$t_s = \sum_{\forall ij} \frac{L_{bij}}{V_{ij}} = \sum_{\forall ij} \frac{1}{V_{ij}}. \tag{15}$$

If we average over all particle paths the mean transit time would be given by

$$t_m = \frac{1}{N_p} \sum_{\forall N_p} \sum_{\forall ij} \frac{1}{V_{ij}} = \left\langle \sum_{\forall ij} \frac{1}{V_{ij}} \right\rangle \equiv M_v(-1). \tag{16}$$

Therefore t_m would scale as $L^{\tau_v(q=-1)}$ where $\tau_v(q) = [f_v(\alpha^*) - q\alpha^*]_{q=df_v/d\alpha|_{\alpha=\alpha^*}}$

We find, using Figs. 3 and 4, that $\tau_v(-1) = 1.67$ in two dimensions and 2.06 in three dimensions. Thus when we plot $C(t)$ vs $t/L^{\tau_v(-1)}$ we obtain a universal curve as shown in Figs. 8 and 9.

IV. CONCLUSIONS

We have studied the multifractal, $f(\alpha)$ spectra of velocities for percolation clusters at threshold in two and three dimensions. The results are consistent with $f(\alpha)=-b\alpha$ for large α with $b\to 0$ as $L\to\infty$. For transport simulations, the velocity histogram should be flux (velocity) weighted, since particles are more likely to reside in the high velocity links. This leads then to a velocity-weighted $f_v(\alpha)$ spectrum that scales as $-b_v\alpha$ for large α with $b_v\to 1$ for $L\to\infty$. This new scaling means that the first moment of the transit-time distribution is well defined.

We confirm this analysis through particle-tracking simulations of advective-dominated transport. The scaling of $f_v(\alpha)$ is consistent with a velocity probability histogram $P_v(V)\sim V^{b_v-1}dV$ or a transit time probability distribution across a link of the form $\psi(t)\sim t^{-1-\beta_v}dt$ with $\beta_v=b_v$. From CTRW theory this leads for $1<\beta_v<2$ to a linear scaling of mean position with time, a standard deviation scaling $\sigma(t)\sim t^{(3-\beta_v)/2}$ and an outlet concentration $C(t)\sim t^{-1-\beta_v}$. Our transport simulations corroborate these scaling laws.

Finally we show that the outlet concentration $C(t)$ collapses onto a universal curve when plotted against $t/L^{\tau_v(-1)}$ where $\tau_v(q)$ is the scaling of the qth moment of the flux weighted velocity distribution.

ACKNOWLEDGMENT

The authors thank the Imperial College Consortium on Pore-Scale Modelling for financial support.

[1] B. B. Mandelbrot, J. Fluid Mech. **62**, 331 (1974).
[2] D. Stauffer and A. Aharony, *Introduction to Percolation Theory*, 2nd ed. (Taylor and Francis, London, 1994).
[3] L. Niemeyer, L. Pietronero, and H. J. Wiesmann, Phys. Rev. Lett. **52**, 1033 (1984).
[4] H. J. Herrmann, Phys. Lett., C **136**, 153 (1986).
[5] S. Havlin and D. Ben-Avraham, Adv. Phys. **36**, 695 (1987).
[6] H. E. Stanley and A. Coniglio, Phys. Rev. B **29**, 522 (1984).
[7] M. Sahimi, Transp. Porous Media **13**, 3 (1993).
[8] L. de Arcangelis, A. Coniglio, and S. Redner, Phys. Rev. B **36**, 5631 (1987).
[9] G. G. Batrouni, A. Hansen, and B. Larson, Phys. Rev. E **53**, 2292 (1996).
[10] M. Barthelemy, S. V. Buldyrev, S. Havlin, and H. E. Stanley, Phys. Rev. E **61**, R3283 (2000).
[11] D. J. Bergman and D. Stroud, Solid State Phys., Adv. Res. Appl. **46**, 147 (1992).
[12] E. Lopez, S. V. Buldyrev, N. V. Dokholyan, L. Goldmakher, S. Havlin, P. R. King, and H. E. Stanley, Phys. Rev. E **67**, 056314 (2003).
[13] L. de Arcangelis, S. Redner, and A. Coniglio, Phys. Rev. B **31**, 4725 (1985).
[14] R. Rammal, C. Tannous, P. Breton, and A.-M. Tremblay, Phys. Rev. Lett. **54**, 1718 (1985).
[15] T. C. Halsey, M. H. Jensen, L. P. Kadanoff, I. Procaccia, and B. I. Shraiman, Phys. Rev. A **33**, 1141 (1986).
[16] L. de Arcangelis, S. Redner, and A. Coniglio, Phys. Rev. B **34**, 4656 (1986).
[17] G. Di Donato, E. O. Obi, and M. J. Blunt, Geophys. Res. Lett. **30**, 10 (2003).
[18] A. Aharony, R. Blumenfeld, and A. B. Harris, Phys. Rev. B **47**, 5756 (1993).
[19] B. Kahng, Phys. Rev. Lett. **64**, 914 (1990).
[20] G. G. Batrouni, A. Hansen, and S. Roux, Phys. Rev. A **38**, 3820 (1988).
[21] H. Scher and M. Lax, Phys. Rev. B **7**, 4491 (1973).
[22] B. Berkowitz and H. Scher, Phys. Rev. Lett. **79**, 4038 (1997).
[23] B. Berkowitz, G. Kosakowski, G. Margolin, and H. Scher, Ground Water **39**, 593 (2001).
[24] M. E. J. Newman and R. M. Ziff, Phys. Rev. E **64**, 016706 (2001).
[25] B. A. Galler and M. J. Fisher, J. Commun. **7**, 301 (1964).
[26] K. Stüben, J. Comput. Appl. Math. **128**, 281 (2001).
[27] M. E. Rhodes and M. J. Blunt, Water Resour. Res. **42**, W04501 (2006).
[28] M. Sahimi, B. D. Hughes, L. E. Scriven, and H. Ted Davis, Chem. Eng. Sci. **41**, 2103 (1986).
[29] P. Grassberger, Physica A **262**, 251 (1999).
[30] T. Nagatani, J. Phys. A **19**, L1165 (1986).
[31] A. Coniglio, J. Phys. A **15**, 3829 (1982).
[32] E. Duering and D. J. Bergman, J. Stat. Phys. **60**, 363 (1990).
[33] B. Berkowitz and H. Scher, Phys. Rev. E **57**, 5858 (1998).
[34] B. Berkowitz, H. Scher, and S. E. Silliman, Water Resour. Res. **36**, 1371 (2000).
[35] M. Shlesinger, J. Stat. Phys. **10**, 421 (1974).
[36] G. Margolin and B. Berkowitz, Phys. Rev. E **65**, 031101 (2002).
[37] B. Berkowitz, A. Cortis, M. Dentz, and H. Scher, Rev. Geophys. **44**, RG2003 (2006).